Minimizing residual vibrations and cross-talk for inkjet printheads using ILC designed simplified actuation pulses

M.B. Groot Wassink [*] ***and O.H. Bosgra*** [*] ***and S.H. Koekebakker*** [**] ***and M. Slot*** [**]
[*] ***Delft University of Technology, Mekelweg 2, 2628 CD Delft, The Netherlands***
[**] ***Océ-Technologies B.V., P.O. Box 101, 5900 MA Venlo, The Netherlands***

Abstract
The attainable performance of inkjet printheads is severely limited by residual vibrations and cross-talk. Both effects are inseparably linked with the actuation of an ink channel. Residual vibrations occur each time a droplet has been jetted and, while actuating a channel, fluid-mechanics in neighboring channels are excited also. These phenomena affect the performance negatively, e.g. in terms of drop-consistency and achievable jetting frequencies. Previous work has shown that Iterative Learning Control (ILC) can be applied to design input wave forms (pulses) that leave the droplet formation undisturbed while minimizing these operational issues. However, the resulting pulses are usually too complex to be implemented on the Application Specific Integrated Circuit (ASIC) of a printhead. In this paper, the ILC control framework is adjusted with a modified algorithm that allows for the design of pulses with predefined complexity. It is demonstrated that this modified ILC using only piece-wise affine command signals operates without a severe loss of performance compared to unconstrained ILC. This paper shows the modeling required for ILC, the design of the controller, and the accompanying experimental results that show the minimization of residual vibrations as well as cross-talk.

Introduction
Inkjet technology ([1]) counts as an important manufacturing technology serving a wide variety of markets, see e.g. [2, 3, 4, 5]. Its popularity as manufacturing technology is closely related to its unique ability to deposit various types of materials on a substrate in certain patterns. Though the performance criteria imposed by today's applications are quite tight already, future performance requirements will be even more challenging. However, the attainable performance is limited by two operational issues that are generally encountered, namely residual vibrations and cross-talk, as discussed in the next Section.

Iterative Learning Control (ILC) is a well-known control strategy for systems that operate repetitively in time, see e.g. [6, 7], such as an inkjet printhead. Though ILC has proven its value in many areas such as robotics ([8]), chemical batch processing ([9]), and servo systems ([10]), its application in the field of inkjet technology was formerly unprecedented. In [11] and [12], lifted ILC ([10, 13]) has been successfully applied to an inkjet printhead to minimize residual vibrations and cross-talk, respectively. The resulting actuation pulses, however, are usually too complex to be implemented on the Application Specific Integrated Circuits (ASIC) of inkjet printheads. For that, it is required that the actuation pulse is constructed by linearly interpolating between as few as possible switching points in time and amplitude. Consequently, an actuation pulse results that consists of a certain number of piece-wise affine parts.

For the design of such extremely simplified actuation pulses within the ILC framework several strategies varying in complexity can be followed. To start with, given the number of switching instances a non-linear optimization problem can be formulated that determines the switching instances in time and amplitude, e.g. see [14]. Interpolation between those points then gives the actuation pulse. However, formulation within an ILC framework is not trivial and the computational complexity makes it unsuitable for implementation on an inkjet printhead. Second, by utilizing a certain set of basis functions the non-linear optimization problem can be transformed into a linear optimization problem within the ILC framework, see e.g. [15, 16]. However, since a high number of basis functions is usually needed to obtain reasonable performance, quite complex actuation pulses result that still are infeasible for ASIC implementation. In this paper, we therefore propose a modified ILC algorithm that utilizes an optimized basis for the construction of actuation signals. This basis is optimized based on known limitations concerning the implementation on an ASIC and physical insight in the working of an inkjet printhead. It is shown that while restraining the complexity of the resulting actuation pulses, the effect of residual vibrations and cross-talk can be minimized without severe loss of performance compared to the unconstrained implementation of MIMO ILC.

This paper is organized as follows. First, a system description is provided. Second, experimental modeling of the system is shortly addressed. The next section deals with the MIMO ILC control framework. Also, the modified lifted ILC algorithm is discussed. Subsequently, the experimental results are presented. Finally, the conclusions and an outlook on future work are given.

System description
A schematic side view of a channel of an inkjet printhead is depicted in Fig. 1. It consists of a channel of several millimeters, a nozzle, and a piezo-unit (both actuator and sensor). Typically, around 75 npi are integrated in an array that forms a printhead. To fire a droplet, a trapezoidal pulse is provided to the piezo-unit. Then, ideally, the following occurs. To start with, a negative pressure wave is generated in the channel by enlarging the volume in the channel (step 1). This pressure wave splits up and propagates in both directions (step 2). These pressure waves are reflected at the reservoir that acts as an open end and at the nozzle that acts

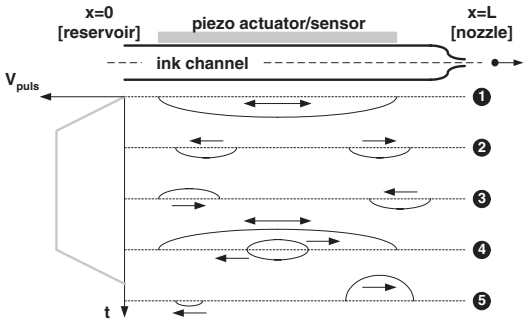

Figure 1. *A schematic view of an inkjet channel and its working principle*

as a closed end (step 3). Note that the negative pressure wave reflecting at the nozzle results in the retraction of the meniscus in the nozzle. Next, by decreasing the channel's volume to its original value a positive pressure wave is superposed on the reflected waves exactly when they are located in the middle of the channel (step 4). Consequently, the wave traveling towards the reservoir is canceled whereas the wave traveling towards the nozzle is amplified such that it is large enough to result in a droplet (step 5).

Two major operational issues are associated with current inkjet printhead designs. First, the actual system deviates from the described ideal representation with respect to the residual pressure waves. After the droplet ejection after around 25 μs, it usually takes an additional 150 μs for these residual vibrations to completely damp out. After approximately 100 μs, they are sufficiently damped to jet the next droplet. Consequently, the jetting frequency is restricted to 10 kHz. Second, if an ink channel is actuated, the fluid-mechanics of neighboring channels are excited as well. This occurs either via pressure waves traveling via the reservoir (acoustical cross-talk) or via the structure itself (structural cross-talk). Structural cross-talk originates mainly from the fact that all piezo-units are connected to the same substrate: deformation of one piezo-unit induces a deformation of the neighboring units. For a more detailed description one is referred to [11, 12].

As explained in [18], the piezo-unit is concurrently used as actuator and sensor. Physically, it senses the force that results from the pressure distribution in the channel acting on the piezo's surface that borders the channel. This force creates a charge on the piezo-unit. Since only changes in charge are measured, in fact the time derivative of the instantaneous present force is sensed. Furthermore, since the resulting voltage drop of this current over a resistance is measured, we have that a voltage is the resulting sensor signal. For the remainder of this paper, it is assumed that the operation of a printhead is linear. In [11], it has been demonstrated that despite the non-linear effect of the jetting of a droplet the printhead system indeed behaves linearly for the control purpose in mind.

System modeling

For the implementation of ILC, an array of two channels are considered. The accompanying transfer functions from the piezo actuator to the piezo sensor are denoted as:

$$\begin{bmatrix} y_A \\ y_B \end{bmatrix} = \begin{bmatrix} H_A(j\omega) & H_{AB}(j\omega) \\ H_{BA}(j\omega) & H_B(j\omega) \end{bmatrix} \begin{bmatrix} u_A \\ u_B \end{bmatrix} \quad (1)$$

where u_A, u_B, y_A, and y_B are the Fourier transforms of the inputs and outputs, respectively. In this paper, it is assumed that all channels are identical, such that only one diagonal and one off-diagonal term in (1) are to be identified, since $H_A(j\omega) = H_B(j\omega)$ and $H_{AB}(j\omega) = H_{BA}(j\omega)$. To that purpose, experimental modeling is utilized. A pseudo sine-sweep was used to identify the accompanying frequency response functions (FRF), see Fig. 2 and 3 for the diagonal and off-diagonal term, respectively. Note that the measured transfer functions depicted in Fig. 2 and 3 include among other things the piezo amplifier and a low-pass filter with a cut-off frequency of 500 kHz. The latter is used to eliminate the high-frequent behavior of the piezo-unit that has its first resonance frequency around 1 MHz. The amplifier and low-pass filter cause a significant phase lag at high frequencies. The resonance frequencies visible in Fig. 2 and 3 can be interpreted as the occurring standing wave in an inkjet channel and its higher order modes. Note that these resonance modes are highly damped.

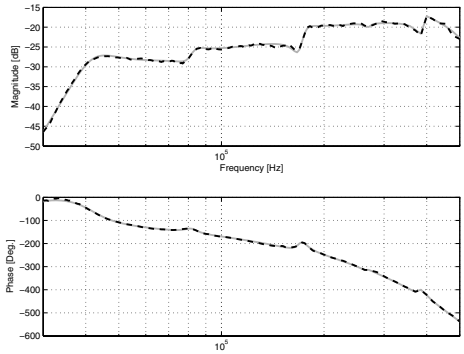

Figure 2. *Frequency Response Function of H_A (H_B) from the piezo actuator to the piezo sensor; FRF (black dotted) and model (gray)*

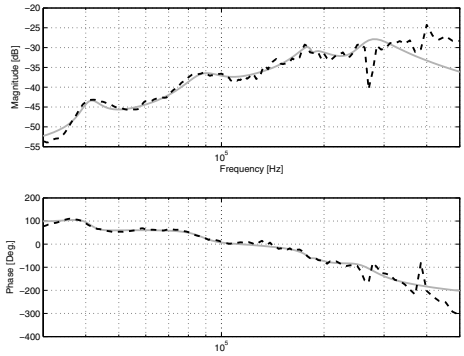

Figure 3. *Frequency Response Function of H_{AB} (H_{BA}) from the piezo actuator to the piezo sensor; FRF (black dotted) and model (gray)*

To obtain linear time invariant models of both measured transfer functions, weighted Output Error (OE) least-squares approximations were used, see [19]. For the diagonal terms $H_A(j\omega)$ and $H_B(j\omega)$, the resulting 16th order model is depicted in Fig. 2. For

the off-diagonal terms $H_{AB}(j\omega)$ and $H_{BA}(j\omega)$, the resulting 14th order model is depicted in Fig. 3. The fitted transfer function for the diagonal terms is quite accurate over the whole frequency range. For the off-diagonal terms, the fit is reasonably accurate up to 250 kHz. To assess the quality of both models, it has been validated using measured sensor signals, see Fig. 4 and 5. These sensor signals are the result of actuating a channel with a standard trapezoidal pulse at a jetting frequency of 10 kHz. Based on Fig. 4 and 5, we conclude that the dynamics are modeled satisfactorily. Despite the modeling errors that are present, the obtained experimental model forms a suitable starting point for ILC. The online ILC controller in combination with the actual system can handle these model inaccuracies quite well, as will be demonstrated in the subsequent sections. Finally, note that the sensor signal of Fig. 5 oscillates in anti-phase to the sensor signal of Fig. 4. This corresponds to the fact that a decrease of one channel induces an increase of its neighboring channels and provides a physical explanation of the obtained sensor signals.

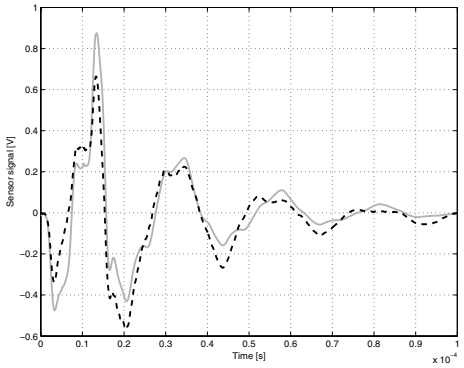

Figure 4. *Sensor signal of an actuated channel resulting from a standard fixed pulse; measured (black) and model response (gray)*

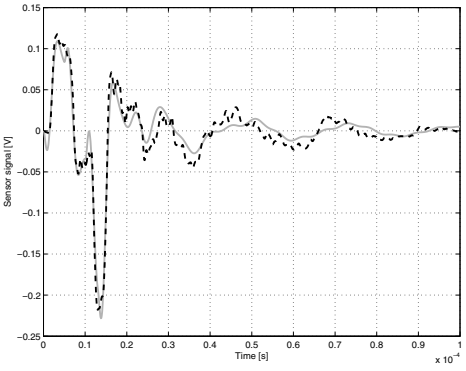

Figure 5. *Sensor signal of a channel neighboring an actuated one resulting from a standard fixed pulse; measured (black) and model response (gray)*

A frequency spectrum of the response to a standard actuation pulse as depicted in Fig. 4 reveals that the dominating frequency of the response equals that of the first eigenfrequency of the ink channel. Apparently, despite the limited magnitude around 45 kHz, the standard actuation pulse is designed such that this mode is excited the most. This provides useful information for the optimization of the basis for the application of ILC, as discussed in the next section.

ILC framework

In this section, the control structure, the formulation of the control goal, and the synthesis and adjustment of the ILC algorithm are discussed.

Control structure

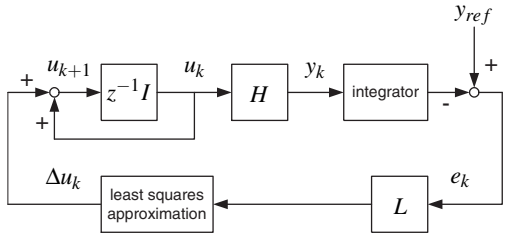

Figure 6. *ILC control structure*

In this paper, use is made of ILC in the lifted setting, see [10, 13]. The accompanying control structure is depicted in Fig. 6. The mapping H is the impulse response matrix of the plant, for an LTI system a lower triangular Toeplitz matrix. The learning matrix, that still has to be designed, is represented by L and may be non-causal and time-varying. z^{-1} is one trial delay operator and can be seen as memory block. For a single channel, the trial length N equals 1000 corresponding with the sample rate of 10 MHz and the DOD frequency of 10 kHz. Signal u_k is a vector containing the system's inputs or states of the ILC system. Signal y_k is the system output, and y_{ref} the reference trajectory. e_k is the error output. The update of the system's input is Δu_k and u_{k+1} is the input for the next trial $k+1$. In case of an array of two channels, A and B, the various signals and impulse response matrix are structured as follows:

$$y_k = \begin{bmatrix} y_k^A(0) \\ y_k^B(0) \\ y_k^A(1) \\ y_k^B(1) \\ \vdots \\ y_k^A(N-1) \\ y_k^B(N-1) \end{bmatrix} \quad u_k = \begin{bmatrix} u_k^A(0) \\ u_k^B(0) \\ u_k^A(1) \\ u_k^B(1) \\ \vdots \\ u_k^A(N-1) \\ u_k^B(N-1) \end{bmatrix} \quad e_k = \begin{bmatrix} e_k^A(0) \\ e_k^B(0) \\ e_k^A(1) \\ e_k^B(1) \\ \vdots \\ e_k^A(N-1) \\ e_k^B(N-1) \end{bmatrix} \tag{2}$$

$$H = \begin{bmatrix} h_A(0) & h_{BA}(0) & 0 & 0 & \dots & 0 & 0 \\ h_{AB}(0) & h_B(0) & 0 & 0 & \dots & 0 & 0 \\ h_A(1) & h_{BA}(1) & h_A(0) & h_{BA}(0) & \dots & \vdots & \vdots \\ h_{AB}(1) & h_B(1) & h_{BA}(0) & h_B(0) & \dots & \vdots & \vdots \\ \vdots & \vdots & \ddots & \ddots & \ddots & \vdots & \vdots \\ h_A(N-1) & h_{BA}(N-1) & \dots & \dots & \dots & h_A(0) & h_{BA}(0) \\ h_{AB}(N-1) & h_B(N-1) & \dots & \dots & \dots & h_{AB}(0) & h_B(0) \end{bmatrix} \tag{3}$$

In case of two channels, the signals in (2) have dimension $2N \times 1$. H has dimension $2N \times 2N$. During learning, the following occurs. At the k-th trial, signal u_k is provided to the system, resulting in the integrated output y_k. The output y_k is then subtracted from

the reference y_{ref} to obtain the error e_k. Based on this error, the learning controller computes the adjustments to the input Δu_k that, added to the previous input, forms the input for the next trail u_{k+1}. Finally, as discussed previously, the measured sensor signal represents the derivative of the pressure in the ink channel. If control would be based on that signal, the derivative of the pressure would be controlled. Therefore, the measured output is numerically integrated as can be seen in Fig. 6.

Control goal

The control goal is to minimize the effects of cross-talk while simultaneously damp the residual vibrations. At this point, these control goals are to be translated to suitable reference trajectories for channel A and B. Now, suppose that channel A and B are required to be in the jetting mode and in rest, respectively.

As starting point for the construction of the reference signal for channel A, the response to a standard trapezoidal pulse, see Fig. 4, is used after it has been numerically integrated as explained in the previous section. To accomplish our control goal for channel A, the following procedure is applied. This obtained response consists of two parts. During the first part (0 - 20 μs), the trajectory is maintained such that a droplet of certain predefined properties results. Deviations from this reference trajectory due to both acoustical and structural cross-talk are actively suppressed by the ILC controller. During the second part of the reference trajectory (20 - 100 μs), the fluid-mechanics are brought to a rest as soon as possible after the firing of a droplet causing the residual vibrations to damp. The damping is imposed to take place somehow gradually. This is done to ensure the refill of the nozzle with ink and to avoid too high actuation voltages. Of course, the choice of the reference trajectory should be such that it is realizable by the system. The resulting reference trajectory for channel A is depicted in Fig. 7. The construction of the reference trajectory for channel B is straightforward: to minimize the effect of cross-talk the pressure inside channel B is to kept zero at all times, see Fig. 8.

ILC synthesis

The design of the ILC controller is formulated in terms of the following optimal control problem:

$$J = \sum_{k=1}^{2N} u_k^T H^T Q H u_k + \Delta u_k^T R \Delta u_k \tag{4}$$

Choosing $Q = I$ and $R = \beta I$, the solution to the optimal control problem (4) is:

$$\Delta u_k = -(\beta I + X)^{-1} X u_k \tag{5}$$

with X the stabilizing solution of the DARE:

$$-X(\beta I + X)^{-1} X + H^T H = 0 \tag{6}$$

The solution X to the Riccati equation (6) can be obtained by several methods. For example, the solution can be approximated by:

$$X = H^T H + \beta I \tag{7}$$

For a more detailed description of the ILC synthesis, one is referred to [10].

The resulting ILC controller computes based on the resulting error signal e_k an update Δu_k of the actuation signal u_k. For reasons mentioned in the introduction, the actuation signal (and the update as well) is to be transformed into a simplified signal. Given a number of switching instances that are fixed in time, a nonlinear least-squares algorithm ([21, 22]) is used to approximate the update Δu_k. The switching instances are chosen such that the first eigenmode of the ink channel can be effectively damped by the ILC algorithm. As discussed during the experimental modeling, since this first eigenmode is dominant in the response this is a suitable choice. If the actuation is changed such that other modes become dominant, the switching instances should be adjusted accordingly. For the inkjet printhead, twelve switching instances are chosen, see Fig. 9 and 10. Note that omitting this projection step, the unconstrained lifted ILC framework is obtained.

Experimental implementation

To compare the performance of the proposed approach with unconstrained ILC, both are implemented on the experimental setup. As discussed previously, channel A and B are required to be in the jetting mode and in rest, respectively. The accompanying reference trajectories for channel A and B are depicted in Fig. 7 and 8, respectively. After both ILC configurations have completed their learning, the resulting signals are compared. The resulting sensor signal from the standard trapezoidal and both learned ILC actuation pulses are shown in Fig. 7 and 8 for channel A and B, respectively. The accompanying actuation pulses are depicted in Fig. 9 and 10. Finally, the cumulative power spectrum (CPS) of the resulting error signal of the standard and both learned ILC actuation pulses of channel A and B are depicted in Fig. 11 and 12.

Based on Fig. 7 and 8, it is concluded that the reference trajectories are attained quite well. Though the tracking performance of the unconstrained ILC pulse is slightly better than the constrained ILC pulse, differences are small. This is confirmed by the great resemblance of the accompanying actuation pulses and the CPS of both signals. Apparently, the proposed modified ILC algorithm does not induce a severe loss of performance. In addition, the resulting actuation pulses for both channels are well suited for implementation on the ASICs of inkjet printheads.

Conclusions and outlook

In this paper, a modified ILC algorithm for the construction of simplified actuation pulses for an inkjet printhead has been proposed. It has been shown that upon using the accompanying ILC framework, extremely simplified actuation pulses can be designed that simultaneously minimize the residual vibrations and cross-talk. Also, it is demonstrated that the attained performance using the simplified actuation pulses approximates that of the standard ILC actuation pulses. Finally, the simplified actuation pulses can easily be implemented on an ASIC such that the barrier for implementation of ILC on inkjet printhead has practically been lifted.

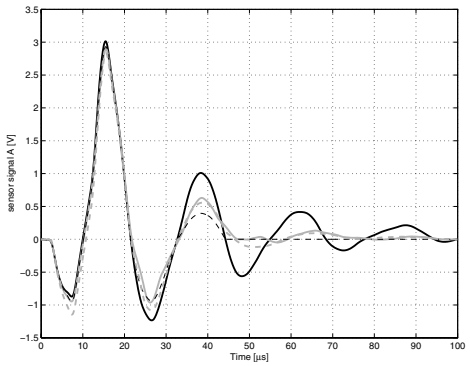

Figure 7. *Integrated sensor signal of channel A; without ILC (black), with constrained ILC (gray), with ILC (gray dotted), and chosen reference trajectory (black dotted)*

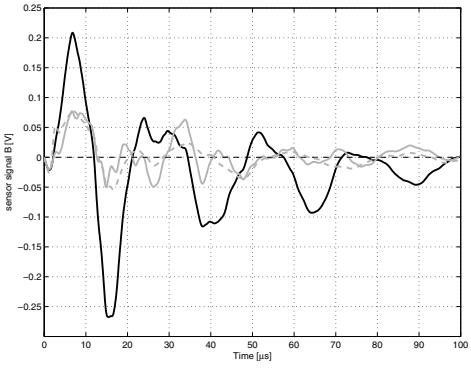

Figure 8. *Integrated sensor signal of channel B; without ILC (black), with constrained ILC (gray), with ILC (gray dotted), and chosen reference trajectory (black dotted)*

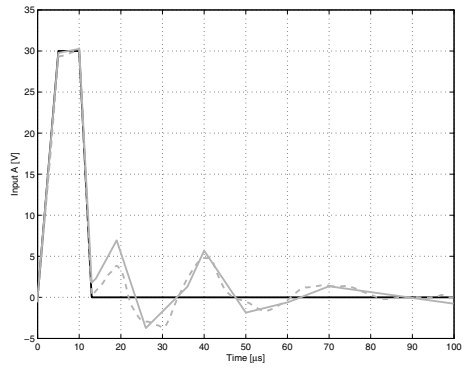

Figure 9. *Actuation pulse for channel A; standard trapezoidal (black), the resulting constrained ILC pulse (gray), and the ILC pulse (gray dotted)*

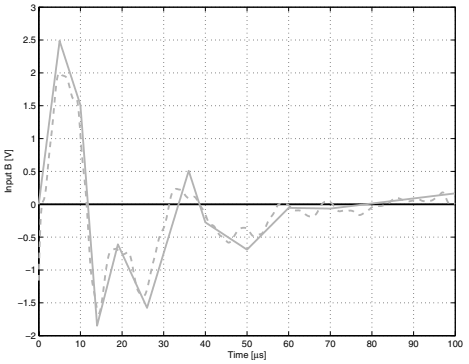

Figure 10. *Actuation pulse for channel B; standard trapezoidal (black), the resulting constrained ILC pulse (gray), and the ILC pulse (gray dotted)*

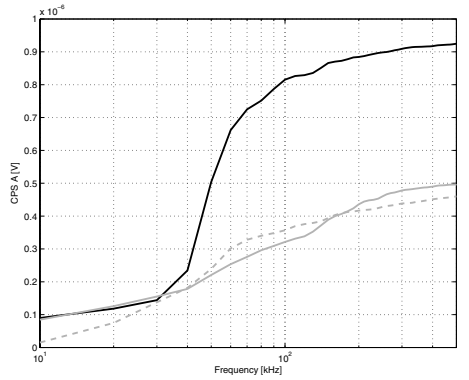

Figure 11. *Cumulative power spectrum of the error signal of channel A; standard trapezoidal (black), constrained ILC pulse (gray), and ILC pulse (gray dotted)*

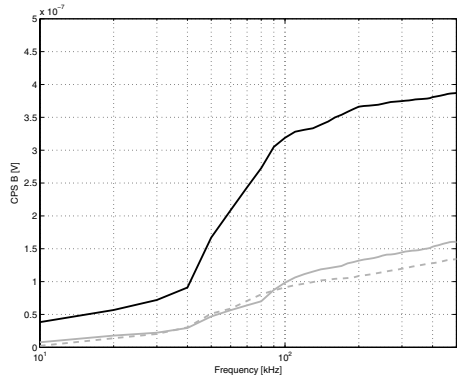

Figure 12. *Cumulative power spectrum of the error signal of channel B; standard trapezoidal (black), constrained ILC pulse (gray), and ILC pulse (gray dotted)*

In the future, further refinement of the proposed algorithm and the choice of the the switching instances are to be investigated.

Acknowledgments

The authors are grateful to Océ-Technologies B.V. for their support of the research reported here.

References

[1] S.F. Pond, Inkjet technology and product development strategies, *Torrey Pines Research*, 2000.

[2] M. Hiddink, Inkjet Printed Polymer OLED Displays for Television Application, *in Proc. International Display Manufacturing Conf.*, Taipei, Japan, 2005.

[3] J.G.V. Scott, Digital printing for printed circuit boards, *Circuit World*, vol 31, no. 4, pp. 34-41, 2005.

[4] J. Noolandi et al., Towards a Neurotransmitter-Based Retinal Prosthesis Using an Inkjet Printhead, *Biomedical Microdevices*, vol 5, no. 3, pp. 195-199, 2003.

[5] X. Zhao et al., Ink-jet printing of ceramic pillar arrays, *Journal of Materials Science*, vol. 37, no. 10, pp. 1987-1992, 2002.

[6] K.L. Moore, *Itertive Learning Control for Deterministic Systems*, Advances in Industrial Control. Springer Verlag, London, 1993.

[7] R.W. Longman, Iterative Learning Control and Repetitive Control for Engineering Practice, *International Journal of Control*, vol. 73, pp. 930-954, 2000.

[8] A. Tayebi, Adaptive iterative learning control for robot manipulators, *Automatica*, vol. 40, pp. 1195-1203, 2004.

[9] K.S. Lee, S.H. Bang, S. Yi, J.S. Son, and S.C. Yoon, Iterative learning control of heat-up phase for a batch polymerization reactor, *Journal of Process Control*, vol. 6, no. 4, pp. 255-262, 1996.

[10] B.G. Dijkstra, O.H. Bosgra, Extrapolation of optimal lifted system ILC solution with application to a waferstage, *in Proc. American Control Conference*, pp. 2595-2600, Anchorage, USA, 2002.

[11] M.B. Groot Wassink, N.J.M. Bosch, O.H. Bosgra, and S.H. Koekebakker, Enabling higher jetting frequencies for an inkjet printhead using Iterative Learning Control, *in Proc. IEEE Conf. on Contr. Applications*, pp. 791-796, Toronto, Canada, 2005.

[12] M.B. Groot Wassink, O.H. Bosgra, and S.H. Koekebakker, Minimization of cross-talk for an inkjet printhead using MIMO ILC, *in Proc. American Control Conf*, pp. 964-969, Minneapolis, USA, 2006.

[13] R. Tousain, E. van der Meché, and O.H. Bosgra, Design strategies for iterative learning control based on optimal control, *in Proc. IEEE Conf. on Dec. and Control*, pp. 4463-4468, Orlando, USA, 2001.

[14] V. Hatzikos, J. Hätönen, and D.H. Owens, Genetic Algorithms in norm-optimal and non-linear iterative learning control, *Int. J. Control*, Vol. 77, no. 2, pp. 188-197, 2004.

[15] M.Q. Phan and J.A. Frueh, Learning Control for Trajectory Tracking using Basis Functions, *in Proc. Conf. on Decision and Control*, pp. 2490-2492, Kobe, Japan, 1996.

[16] D. Gorinevsky, D.E. Torfs, and A.A. Goldenberg, Learning Approximation of Feedforward Control Dependence on the Task Parameters with Application to Direct-Drive Manipulator Tracking, *IEEE Transactions on Robotics and Automation*, Vol. 13, no. 4, pp. 567-581, 1997.

[17] S. Gunnarsson and M. Norrlöf, On the design of ILC algorithms using optimization, *Automatica*, Vol. 37, pp. 2011-2016, 2001.

[18] European Patent 1 378 360 A1

[19] R. Schrama, *Approximate identification and control design with application to a mechanical system*, PhD thesis, Delft University of Technology, 1994.

[20] J.F. Dijksman, Hydrodynamics of small tubular pumps, *Journal of Fluid Mechanics*, vol. 139, pp. 173-191, 1984.

[21] K. Levenberg, A Method for the Solution of Certain Problems in Least Squares, *Quarterly Applied Mathematics II*, pp. 164-168, 1944.

[22] D. Marquardt, An Algorithm for Least-squares Estimation of Nonlinear Parameters, *SIAM Journal Applied Mathematics*, Vol. 11, pp. 431-441, 1963.

Author Biography

Matthijs Groot Wassink (1978) received his MSc degree in mechanical engineering from Delft University of Technology, the Netherlands, in 2002. For his research on 'Linear Parameter Varying Control for a Wafer Stage' he was awarded the Unilever Research Prize. He worked as research engineer for Philips Center for Industrial Technology in Eindhoven, the Netherlands. Currently, he conducts his PhD research at Delft University of Technology in close collaboration with Océ-Technologies B.V. in Venlo, the Netherlands.